Article

The Effect of W, Cr, Mo Content on the Microstructure and Mechanical Properties of the Weld Interface of TiC Cermet and Low-Carbon Steel

Wei Wei [1,2], Zhiquan Huang [1], Haiyan Zhang [1] and Shaokang Guan [2,*]

1   Zhengzhou Research Institute of Mechanical Engineering, Zhengzhou 450000, China; weiw@zrime.com.cn (W.W.); tehanshiyanshi@hotmail.com (Z.H.); trunks.ww@163.com (H.Z.)
2   School of Material Science & Enginreering, Zhengzhou University, Zhengzhou 450000, China
*   Correspondence: skguan@zzu.edu.cn

Abstract: In this study, the influence of W, Cr, and Mo on the microstructure and mechanical properties of the arc-welded interface of TiC cermet and low-carbon steel was investigated. MIG arc welding was employed to deposit muti-alloyed low-carbon steel flux-cored wire onto the surface of the TiC cermet to create the arc-welded interface. Analysis of the microstructure, phase composition, and shear fracture of the interface were conducted by OM (optical microscopy), SEM (scanning electron microscope), EMPA (Electron Probe X-ray Micro-Analyzer), and XRD (X-ray diffraction) methods. The results indicate that the order of influence on the performance of the welded interface is perceived as Cr > W > Mo. The preferred ratio of element content is W at 1.0 wt.%, Cr at 0.5 wt.%, and Mo at 2.0 wt.%. During the arc-welding process, W and Mo formed a rim structure of TiC particles to inhibit the dissolution of TiC particles, while Cr formed dispersed carbides in the bonding phase. The synergistic impact of these components resulted in the simultaneous enhancement of both the TiC particles and the bonding phase. This led to a significant increase in the shear strength of the TiC cermet welded interface to 787 MPa, marking an 83% improvement compared to the welded interface without reinforcement, which exhibited a shear strength of 430 MPa.

Keywords: TiC cermet; arc welding; multi-alloy strengthening; interface; shear strength

1. Introduction

TiC cermet is primarily composed of TiC or Ti(C,N) as the main components, with elements such as Ni, Mo, and Fe used as the main elements to create the bonding phase. Compared to WC particles, TiC particles have the characteristics of low density ($4.93 \, \mathrm{g/cm^3}$), high hardness (3200 HV) [1], and stable properties. The literature shows that the wear resistance of the matrix reinforced with TiC is increased by 1–2 orders compared to non-reinforcement [2]. TiC cermet inherits the advantages of both cemented carbide and steel, combining the high hardness and wear resistance of cemented carbide with the machinability, heat treatability, and forgeability of steel, demonstrating excellent overall performance [3–6]. However, the manufacturing cost of TiC cermet is relatively high, the manufacturing conditions are strict, and there are difficulties in producing large-sized parts, leading to its limited application range due to its expensive price [7,8]. Therefore, the majority of successful applications depend on the bond between the TiC cermet and the metal matrix.

The weldability of TiC cermet was investigated based on previous research achievements [9]. A Gleeble simulation was employed to occur the heat affect zone of TiC cermet, and the microstructure and mechanical properties results showed that TiC cermet has a stable chemical and physical properties during the welding heat-input process; hence, the TiC cermet has certain weldability. The research conducted focused on identifying the most suitable weld metal for welding TiC cermet. Various alloyed welding materials were

used to study the microstructure and mechanical properties of the welded interface in TiC cermet. The findings revealed that low-carbon alloy steel with ferrite is the most suitable welding material for arc welding TiC cermet. This suggests that using this specific material can result in improved weld quality and overall performance of the welded interface [10]. Therefore, the reinforcement of the bond between the TiC cermet and the metal matrix is being valued. Lee [11] studied a TiC metal ring containing Mo_2C and WC, and this specific microstructure inhibited the diffusion of carbides in the core (TiC) and edge (Ti, Mo, or W). This phenomenon combines the effects of solid-state diffusion processes (inner edge) and dissolution–precipitation mechanisms (outer edge). The addition of W to TiC gives it a smaller lattice constant compared to other elements, resulting in slightly larger lattice vibrations [12]. Lin [13] investigated the effects of chromium on TiC cermet; the results show that with an increase in the chromium content, the porosity of sintered samples increases and the TRS of the sample gradually decreases, with the hardness firstly increasing and then decreasing a little.

The literature shows that TiC cermet has certain weldability and that low-carbon alloy steel is most suitable for arc welding, while W, Cr, and Mo alloy elements can inhibit the decomposition of TiC particles and improve the strength of sintering test samples in the liquid sintering process of TiC steel cemented carbide. In this article, the MIG welding method was employed to obtain weld interfaces between low-carbon steel and TiC cermet. W, Cr, and Mo were added to the low-carbon steel weld material to enhance the interface. The analysis of the microstructure and mechanical properties of the joints was conducted to identify the preferred Cr, W, and Mo content.

2. Materials and Methods

Materials

An orthogonal experimental table of three factors and four levels was adopted to investigate the effects of W, Cr, and Mo on the TiC cermet welding interface. The low-carbon steel welding wire and the TiC cermet used in this study were produced by Zhengzhou Research Institute of Mechanical Engineering Co., Ltd., Zhengzhou, China, and the chemical and mechanical properties tested following «GB/T 223» [14] «GB/T 40388» [15] and «ASTM E1269-11» [16] standards, respectively. The results are shown in Table 1.

Table 1. Chemical (wt.%) and mechanical properties of weld metal and TiC cermet.

	C	Ni	Mn	TiC	Mo	Fe	Shear Strength (MPa)
ZDZC60	0.53	1.78	6.21	39.50	1.31	etc.	469
LCS	0.051	-	0.78	-		etc.	430

The alloys' content levels were set at 0.5 wt.%, 1.0 wt.%, 1.5 wt.%, and 2.0 wt.%. Since the original low-carbon alloy steel contains 0.5 wt.% of Mo, the Mo content was set at 1.0 wt.%, 1.5 wt.%, 2.0 wt.%, and 2.5 wt.%. Table 2 shows the specific experimental arrangement of the orthogonal experimental table with three factors and four levels. The composition of the welded metal and TiC cermet is shown in Table 2. The welding parameters were set as follows: welding current of 270 A, voltage of 27 V, and welding speed of 0.8 cm/s. The microhardness gradients of the joints were obtained by measuring at intervals of 0.1 mm perpendicular to the interface. The morphology of the samples was analyzed by Phoneme XL1 scanning electron microscope (SEM) and EPMA. The phase patent was analyzed by D8 type X-ray diffraction (XRD).

Table 2. Element design.

	W	Cr	Mo
1#	0.5	0.5	1.0
2#	0.5	1.0	1.5
3#	0.5	1.5	2.0
4#	0.5	2.0	2.5
5#	1.0	0.5	1.5
6#	1.0	1.0	1.0
7#	1.0	1.5	2.5
8#	1.0	2.0	2.0
9#	1.5	0.5	2.0
10#	1.5	1.0	2.5
11#	1.5	1.5	1.0
12#	1.5	2.0	1.5
13#	2.0	0.5	2.5
14#	2.0	1.0	2.0
15#	2.0	1.5	1.5
16#	2.0	2.0	1.0

3. Results

The orthogonal experimental analysis was conducted on the samples of low-carbon alloy steel welded with TiC steel cemented carbide, and the analysis of the shear strength data of the low-carbon alloy steel welded with TiC cermet arc welding in the orthogonal experiment is shown in Table 3.

Table 3. Data analysis of shear strength (MPa) of TiC cermet arc-welding interface.

	W	Cr	Mo	Shear Strength (MPa)
1#	0.5	0.5	1.0	746
2#	0.5	1.0	1.5	712
3#	0.5	1.5	2.0	698
4#	0.5	2.0	2.5	765
5#	1.0	0.5	1.5	752
6#	1.0	1.0	1.0	711
7#	1.0	1.5	2.5	773
8#	1.0	2.0	2.0	767
9#	1.5	0.5	2.0	782
10#	1.5	1.0	2.5	646
11#	1.5	1.5	1.0	761
12#	1.5	2.0	1.5	747
13#	2.0	0.5	2.5	751
14#	2.0	1.0	2.0	727
15#	2.0	1.5	1.5	755
16#	2.0	2.0	1.0	714
mean value 1	730.25	757.75	733.00	
mean value 2	750.75	699.00	741.50	
mean value 3	734.00	746.75	743.50	
mean value 4	736.75	748.25	733.75	
MAX	750.75	757.75	743.50	
MIN	730.25	699.00	733.00	
range	20.50	58.75	10.50	

A comparison of the effects of each alloying element on the shear strength of the welded TiC cermet interface reveals that the element Cr has the most significant impact, with a range of 58.75. The maximum mean value is 757.75, corresponding to the level of 0.5 wt.%. The element W has the second most significant impact, with a range of 20.50. Its maximum value is 750.75, corresponding to the level of 1.0 wt.%. The impact of the

element Mo is the least significant, with a range of 10.50. Its maximum value is 743.50, corresponding to the level of 2.0 wt.%. In terms of the shear strength performance, the optimal alloy composition should involve W content of 1.0 wt.%, Cr content of 0.5 wt.%, and Mo content of 2.0 wt.%.

For verification purposes, a welding wire with the optimal alloy composition was prepared. The composition of the weld metal is shown in Table 4.

Table 4. Composition of weld metal (wt.%).

	C	**W**	**Mn**	**Cr**	**Mo**	**Fe**
LCS	0.051	0.95	0.78	0.55	1.94	etc.

The low-carbon alloy steel welding wire, with W, Cr, and Mo alloy element strengthening ratios of 1.0 wt.%, 0.5 wt.%, and 2.0 wt.%, respectively, was used to arc weld the interface of TiC cermet, and the microstructure was observed using SEM. Figure 1 illustrates the microstructure results of the weld interface between the TiC cermet and the welding materials. Remarkably, the interface exhibited successful metallurgical bonding with TiC cermet.
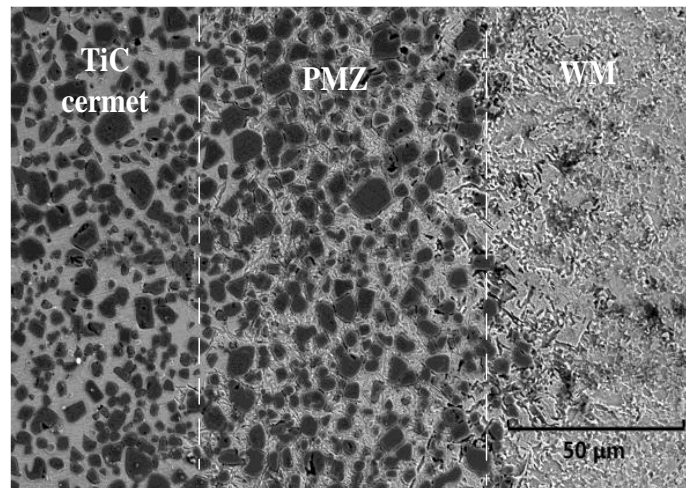

Figure 1. SEM microstructure at the interface.

The arc-welded interface maintains the heat-affected zone (HAZ)–partially melted zone (PMZ)–unmelted zone (UZ)–weld metal (WM) microstructure. The arc-welding interface is observed by SEM, as shown in Figure 1. The TiC cermet and the metal exhibited good metallurgical bonding at the interface, and no microcracks or defects were found at the weld interface compared to the interface welded with γ-Fe or γ-Ni weld metal in previous research [10], indicating good metallurgical bonding between the weld metal and the TiC cermet. A comparison with the analysis of non-alloy-strengthened welding interfaces in [10] reveals that multi-alloy strengthening inhibited the decomposition of TiC particles, resulting in only a small amount of in-situ carbides being formed in the UZ. At the same time, multi-alloy strengthening promotes inter-diffusion between the overlay metal and the TiC cermet, enlarging the PMZ, with a PMZ width of 74 µm, more wild than the width of 20 µm with none strength weld interface [10].

Figure 2 compared the EPMA results of the PMZ between the multi-alloy-strengthened and non-strengthened samples. The microstructure of the PMZ is shown in Figure 2a,b, with the black TiC particle diffusion distributed in the light gray bonding phase. An obvious dark black inner core surrounded by a lighter black rim structure was observed in the TiC particles. While a clear rim distribution of W on the outer layer of the TiC particles was detected in the multi-alloy-strengthened PMZ, the TiC core was similarly surrounded by a W-rich solid-solution carbide phase of Ti-W-C. In contrast, little W was detected in

the non-strengthened PMZ, as shown in Figure 2c,e. During the melting process, the TiC particles dissolved into a solid–liquid phase, in which the mass transport of the carbides are driven by W and Mo, as both W and Mo are strong carbide-forming elements. The formation of the 'core-rim' structure is able to increase the wetting of TiC by the bonding phase in order to improve the bonding strength between TiC particles and the bonding phase. There was no obvious clustering of Cr in either sample; as shown in Figure 2d,f, the Cr element is dispersed throughout the bonding phase, and no Cr-rich solid-solution carbide rim structure was observed. It can be observed in Figure 2g,i that in both samples there is a noticeable accumulation of Mo on the outer layer of the TiC particles. During the cooling process, a 'core-rim' structure of Mo-rich solid-solution carbide formed the Ti-Mo-C phase as the outer layer rim surrounding the TiC core. This structure is similar to that of TiC particles in sintered TiC cermet [17].
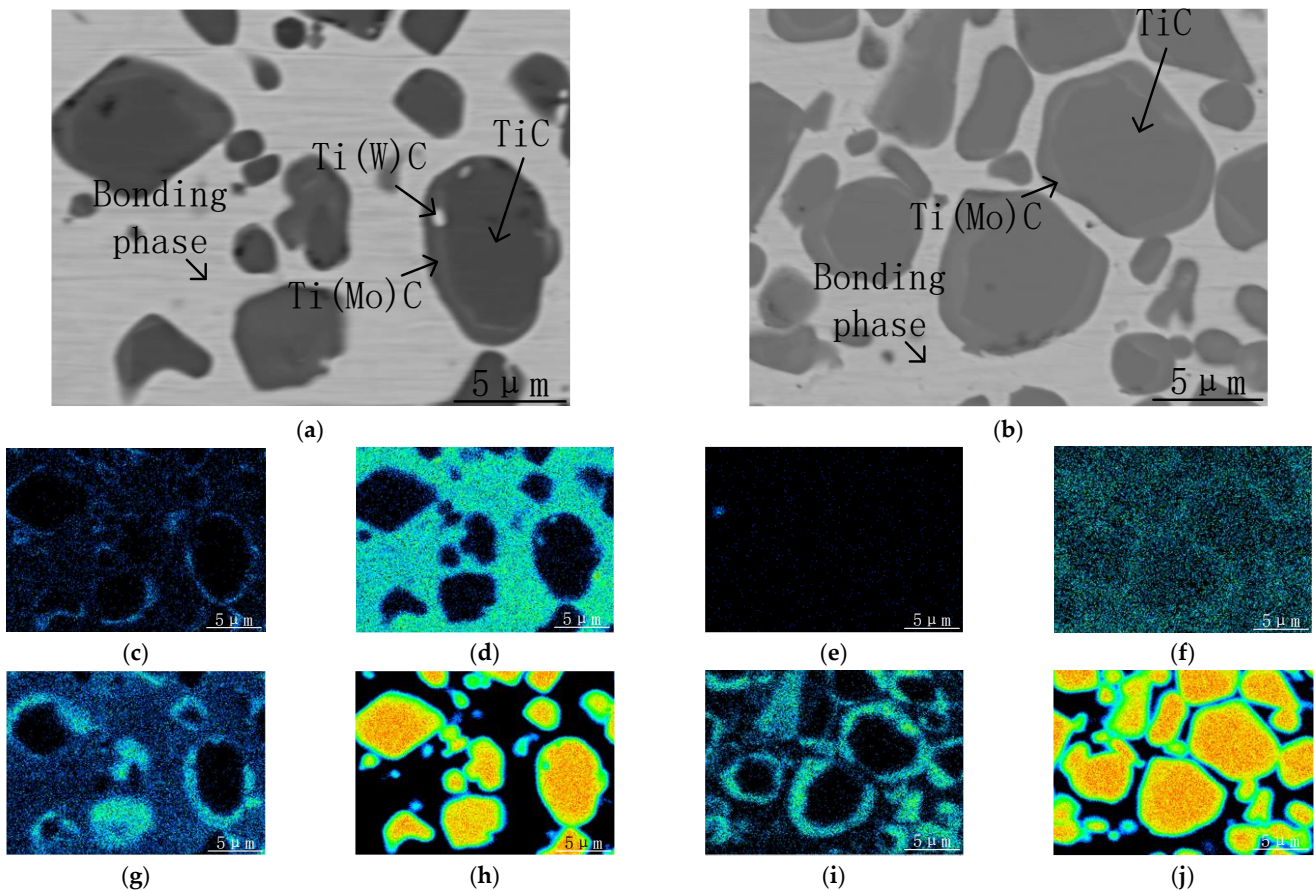

Figure 2. Element distribution in PMZ. (**a**) Multi-alloy strengthened microstructure; (**b**) non-strengthened microstructure; (**c**) W distribution in (**a**); (**d**) Cr distribution in (**a**); (**e**) W distribution in (**b**); (**f**) Cr distribution in (**b**); (**g**) Mo distribution in (**a**); (**h**) Ti distribution in (**a**); (**i**) Mo distribution in (**b**); (**j**) Ti distribution in (**b**).

Arc welding is a rapid heating and cooling metallurgical reaction process. During the welding process, TiC particles decompose to release C and Ti. In this experiment, due to insufficient time for the C to diffuse into the bonding phase, a metallurgical reaction occurred on the surface of the TiC particles, leading to the formation of a 'core-rim' structure, with the TiC core surrounded by a Ti-(Mo,W)-C phase. While there was no Cr rim structure in Figure 2d, as Mo and W are stronger carbide-forming elements than Cr, the characterization reveals the formation of a compound primarily composed of Mo, W, C, and Ti on the surface of TiC particles, which effectively inhibits the melting decomposition of internal TiC particles [18]. Consequently, after the formation of the 'core-rim' structure

primarily composed of Mo, W, C, and Ti, the short amount of C in the bonding phase led to the partial formation of Cr carbide particles and solid-solution strengthening dispersed throughout the bonding phase. XRD analysis of the interface results is shown in Figure 3.
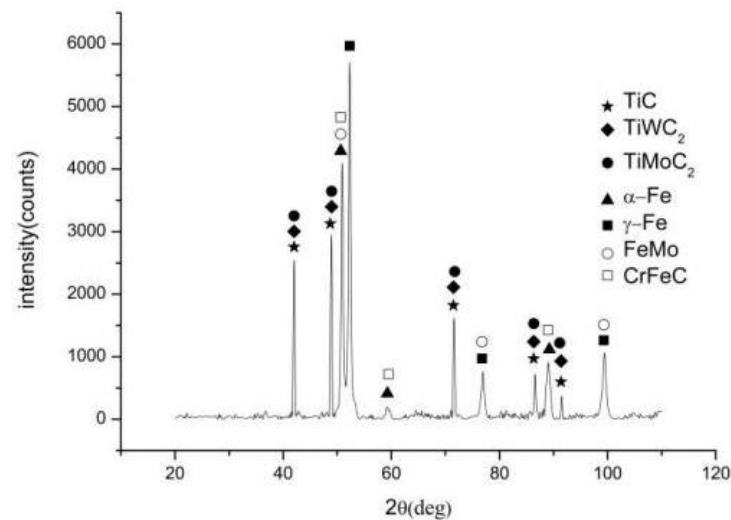

Figure 3. XRD test of the welded interface.

Based on the results shown in Figure 3, the optimal-ratio arc-welded TiC cermet interface contains peaks of TiC, γ-Fe, and α-Fe phases, which is consistent with the phase analysis results of the interface between low-carbon steel and TiC cermet [10]. With the addition of Mo and W, there are peaks of phases containing Ti(Mo,W)C in the interface XRD scan results. Combined with the analysis in Figure 2c,g, a composite carbide of 'core-rim' structure is formed by the Ti(Mo,W)C phase surrounding the TiC particles in the PMZ. The presence of peaks corresponding to Cr-Fe-C, along with the absence of peaks of phases containing Ti-Cr-C, reveals that Cr did not play a role in the formation of the rim structure. Instead, Cr contributed to the formation of carbides with a diffusion distribution in the bonding phase alone with solid-dissolution strengthening.

The shear strength of the interface of the multi-alloy-strengthened low-carbon alloy steel and TiC cermet was tested, and the result was compared with the interface of the TiC cermet arc welded with low-carbon alloy steel welding wire, the non-strengthened arc-welded interface, sintered TiC cermet, and TiC cermet after 6.2 kJ/cm heat input simulation, as shown in Table 5.

Table 5. Verification of the shear strength of TiC cermet interface [9,10].

	Shear Strength (MPa)
Multi-alloy-strengthened	787
Non-strengthened	430
Sintered TiC cermet	469
TiC cermet with 6.2 kJ/cm heat input simulation	584

According to Table 5, the shear strength of the interface significantly increased after being multi-alloy-strengthened compared to other samples. The sample with the optimal ratio had an interface shear strength of 787 MPa, showing a slight improvement compared to the highest value of 782 MPa in the orthogonal experiments (Table 3). Compared to the shear strength of 430 MPa of the non-strengthened interface, an outstanding 83% improvement was occurred through multi-alloy strengthening. When comparing the shear strength of sintered/heat-input-simulated TiC cermet and multi-alloy-strengthened TiC cermet welding interfaces, it was found that the weak point of the weld bond lies on

the TiC cermet side. However, it was also observed that the interface between the two materials exhibits a higher shear strength than the TiC cermet itself. This indicates that the multi-alloy-strengthened TiC cermet may offer improved bonding properties and overall performance. The ratios of the elements with the highest shear strength values in the orthogonal experiments were 1.5 wt.%, 0.5 wt.%, and 2.0 wt.%, respectively, which is essentially consistent with the factor content of the optimal ratio.

Figure 4 shows the SEM image of the shear fracture section of the arc-welded interface after strengthening with W, Cr, and Mo alloy elements. It can be observed that there is no significant change in the morphology of the TiC particle phase at the fracture surface of the sample; the shear fracture section is of quasi-cleavage rupture type. The TiC phase contains many differently oriented cleavage steps that exhibit brittle transgranular fractures, while the bonding phase contains a straight tearing ridge. This is attributed to the metal–ceramic characteristics of the TiC particles [19], indicating a strong metallurgical bond between the TiC particles and the bonding phase at the arc-welded interface. As a result, the plastic deformation characteristics become more obvious as the dimples and tearing ridge on the shear fracture section of the sample increased, including shallow small dimples and a few different-sized equiaxed dimples. These deformations signify an improvement in the shear strength of the arc-welded interface of TiC cermet.
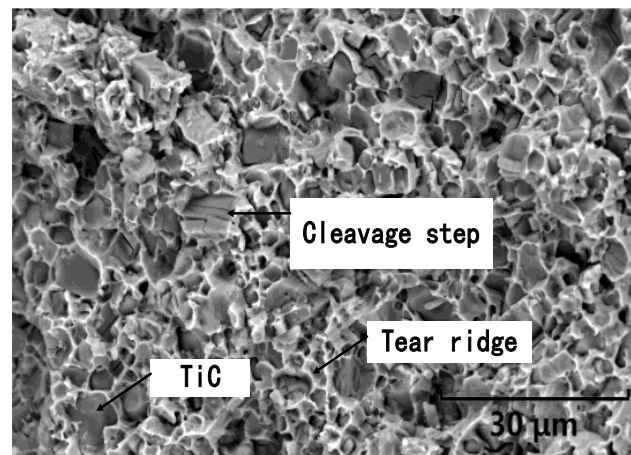

Figure 4. Optimal composition of arc-welded TiC cermet interface fracture.

The fracture section of the samples shows cleavage steps with different orientations. In the shear fracture section, with the diffusion distribution in the bonding phase of Cr carbides and Cr solid-dissolution strengthening in the bonding phase, the toughening dimples of the bonding phase and the tearing ridge of the bonding phase indicate that the TiC cermet bonding phase undergoes plastic deformation before fracturing. The brittle cleavage steps transgranular fractures indicate that during the welding process, TiC particles melted and decomposed, leading to an increase in lattice dislocation, forming carbon-depleted phases, which increased the brittleness of the TiC particles. Hence, secondary cracks were exhibited in the TiC particles. These brittle TiC particles acted as crack initiators, leading to a decrease in the shear strength of the samples. The fracture exhibited quasi-cleavage fractures overall.

Figure 5 illustrates a simplified model depicting the evolution of the microstructure at the interface of low-carbon steel welding material arc welded with TiC cermet following reinforcement with W, Cr, and Mo.

During the welding process, the Ti and C elements in the PMZ formed the shell with the W and Mo elements during the cooling process to inhibit the precipitation of C. Parts of the Cr and C form fine carbides that are distributed in the bonding phase, and part of the Cr contributes to the solid-solution strengthening of the bonding phase.
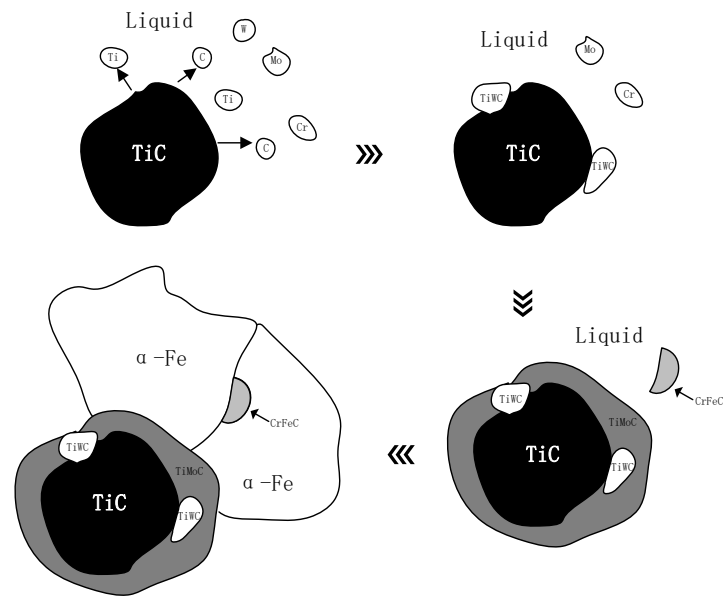
Figure 5. Microstructure evolution of TiC cermet arc welding.

4. Discussion

According to the 'core-rim' theory [20], during the high-temperature stage of welding, TiC particles are distributed in a bonding phase consisting of a mixture of ferrite from the weld metal and austenite from the bonding phase of the TiC cermet, while some TiC particles dissolve into the mixed bonding phase. As W and Mo are stronger carbide-forming elements than Cr, during the cooling process, the W initially nucleates with the C on the surface of the TiC particles, then Mo starts to form the carbides surrounding the TiC particles. With most of the Mo and W participating in reactions on the surface of the TiC particles, a Ti(W,Mo)C outer ring structure forms around the surface of the TiC particles [21], which inhibits the dissolution of the TiC particles, while Cr remains in the mixed bonding phase. The difference from the research conclusions lies in the fact that Jin [22] used a liquid-phase sintering method with a long high-temperature duration of up to 240 min, allowing sufficient time for W, Cr, and Mo elements to form a complex three-layer 'core-rim' structure containing TiC-Ti(W,Mo)C-Ti(Cr,Ni)C. However, arc welding is a process of rapid heating and rapid heat dissipation. Within a brief liquid phase, elements cannot fully react on the surface of TiC particles. Therefore, only W and Mo alloys with stronger carbide-forming elements can nucleate with C on the surface of TiC particles, forming the 'core-rim' structure. Simultaneously, a portion of the Cr reacts with a small quantity of C in the bonding phase, leading to the precipitation of chromium carbides at the ferrite grain boundaries. The presence of dispersed chromium carbides in the matrix enhances the overall strength of the samples. However, as the Cr content increases, the presence of carbide inclusions also escalates. This leads to more C being engaged in the reaction with chromium carbides, with the C originating from the dissolution of TiC particles. Consequently, this process ultimately causes brittleness in the TiC particles. The remaining Cr elements undergo solid dissolution to strengthen the bonding phase. Therefore, the combined effects of Cr strengthening the bonding phase and W and Mo inhibiting the TiC particles collectively influence the mechanical properties at the arc-welded interface of TiC cermet.

The following conclusions can be stated:

(1) An L^3_4 orthogonal experiment was carried out to investigate the effects of W, Cr, and Mo on the microstructure and properties of the arc-welded interface of TiC cermet. The order of importance within the experimental range on the interface properties was perceived as Cr > W > Mo.

(2) During the welding process, W and Mo alloy elements formed a 'core-rim' structure around the TiC particles, inhibiting the dissolution, while Cr formed dispersed carbides within the bonding phase. The combined effects of these elements enhanced the shear strength of the arc-welded interface of TiC cermet. The optimal alloy proportions for welding TiC cermet were determined to be W 1.0 wt.%, Cr 0.5 wt.%, and Mo 2.0 wt.%.

(3) The shear strength of the welded interface increased by 83% compared to non-strengthened conditions, significantly enhancing the bonding strength of the arc-welded interface of TiC cermet.

Author Contributions: Conceptualization, W.W. and S.G.; methodology, W.W.; validation, W.W., S.G. and Z.H.; investigation, W.W.; writing—review and editing, W.W.; project administration, W.W. and H.Z. All authors have read and agreed to the published version of the manuscript.

Institutional Review Board Statement: Not applicable.

Informed Consent Statement: Not applicable.

Data Availability Statement: Data are contained within the article.

Conflicts of Interest: The authors declare no conflicts of interest.

References

1. Kalita, V.I.; Radyuk, A.A.; Komlev, D.I.; Mikhailova, A.B.; Alpatov, A.V.; Chueva, T.R.; Gamurar, N.V.; Titov, D.D. TiC–Cr3C2–WC–TiB2–SiC-Based Cermets. *Inorg. Mater. Appl. Res.* **2020**, *11*, 1199–1213. [CrossRef]

2. SAlgodi, J.; Murray, J.W.; Brown, P.D.; Clare, A.T. Wear performance of TiC/Fe cermet electrical discharge coatings. *Wear* **2018**, *402–403*, 109–123. [CrossRef]

3. Sribalaji, M.; Mukherjee, B.; Bakshi, S.R.; Arunkumar, P.; Babu, K.S.; Keshri, A.K. In-situ formed graphene nanoribbon induced toughening and thermal shock resistance of spark plasma sintered carbon nanotube reinforced titanium carbide composite. *Compos. B Eng.* **2017**, *123*, 227–240. [CrossRef]

4. Xue, J.X.; Liu, J.X.; Zhang, G.J.; Zhang, H.B.; Liu, T.; Zhou, X.S.; Peng, S.M. Improvement in mechanical/physical properties of TiC625 ceramics sintered at 1500 °C for inert matrix fuels. *Scr. Mater.* **2016**, *114*, 5–8. [CrossRef]

5. Namini, A.S.; Ahmadi, Z.; Babapoor, A.; Shokouhimehr, M.; Asl, M.S. Microstructure and thermomechanical characteristics of spark plasma sintered TiC ceramics doped with nano-sized WC. *Ceram. Int.* **2019**, *45*, 2153–2160. [CrossRef]

6. Babapoor, A.; Asl, M.S.; Ahmadi, Z.; Namini, A.S. Effects of spark plasma sintering temperature on densification, hardness and thermal conductivity of titanium carbide. *Ceram. Int.* **2018**, *44*, 14541–14546. [CrossRef]

7. Maurya, H.S.; Kollo, L.; Tarraste, M.; Juhani, K.; Sergejev, F.; Prashanth, K.G. Selective Laser Melting of TiC-Based Cermet: HIP Studies. *Trans. Indian Inst. Met.* **2023**, *76*, 565–570. [CrossRef]

8. Maurya, H.S.; Kollo, L.; Juhani, K.; Sergejev, F.; Prashanth, K.G. Effect of preheating and cooling of the powder bed by laser pulse shaping on the microstructure of the TiC based cermets. *Ceram. Int.* **2022**, *48*, 20612–20618. [CrossRef]

9. Wei, W.; Huang, Z.; Zhang, H.; Guan, S. Effect of the Welding Thermal Cycle on the Microstructure and Mechanical Properties of TiC Cermet HAZ Using the Gleeble Simulator. *Coatings* **2023**, *13*, 476. [CrossRef]

10. Wei, W.; Huang, Z.; Zhang, H.; Guan, S. The Influence of Different Alloyed Welding Materials on the Microstructure and Mechanical Properties of Welded Interface in TiC Cermet MIG Welding Bonds. *Mater. Lett.* **2024**, *361*, 135641. [CrossRef]

11. Lee, J.H.; Park, H.K. Microstructural evolution and mechanical properties of TiC-Mo2C-WC-Ni multi-component powder by high energy ball milling. *J. Ceram. Process. Res.* **2021**, *22*, 590–596.

12. Chen, R.; Chen, L.; Wang, L.; Liang, C. Alloying effects of Zr, Nb, Ta, and W on thermodynamic and mechanical properties of TiC based on first-principles calculation. *Nucl. Mater. Energy* **2024**, *38*, 101604. [CrossRef]

13. Lin, T.; Guo, Y.; Wang, Z.; Shao, H.; Lu, H.; Li, F.; He, X. Effects of chromium and carbon content on microstructure and properties of TiC-steel composites. *Int. J. Refract. Met. Hard Mater.* **2018**, *72*, 228–235. [CrossRef]

14. *GB/T 223.54.2022*; Iron, Steel and Alloy—Determination of Nickel Content—Flame Atomic Absorption Spectrometric Method. Standards Press of China: Beijing, China, 2022.

15. *GB/T 40388-2021*; Test Method for Shear Strength of C/C Composites. Standards Press of China: Beijing, China, 2022.

16. *ASTM E1269-11*; Standard Test Method for Determining Specific Heat Capacity by Differential Scanning Calorimetry. ASTM: West Conshohocken, PA, USA, 2018.

17. Jõeleht, M.; Pirso, J.; Juhani, K.; Viljus, M.; Traksmaa, R. The influence of high energy milling and sintering parameters on reactive sintered (Ti, Mo)C–Ni cermets. *J. Alloys Compd.* **2015**, *636*, 381–386. [CrossRef]

18. Li, Y.; Liu, N.; Zhang, X.; Rong, C. Effect of Mo addition on the microstructure and mechanical properties of ultra-fine grade TiC-TiN-WC-Mo$_2$C-Co cermets. *Int. J. Refract. Metals Hard Mater.* **2008**, *26*, 190–196. [CrossRef]

19. Zhai, W.; Zhu, Z.; Zhou, W.; Nai, S.M.L.; Wei, J. Selective laser melting of dispersed TiC particles strengthened 316L stainless steel. *Compos. Part B Eng.* **2020**, *199*, 108291. [CrossRef]

20. Guan, Y.; Huang, Q.; Peng, Y.; Liu, X.; Kong, Y.; Mao, H. Phase-field simulation of core-rim structure at the early sintering stage in TiC-WC-Ni cermet. *Calphad* **2024**, *84*, 102660. [CrossRef]

21. Xiong, H.; Wu, Y.; Li, Z.; Gan, X.; Zhou, K.; Chai, L. Comparison of Ti(C, N)-based cermets by vacuum and gas-pressure sintering: Microstructure and mechanical properties. *Ceram. Int.* **2018**, *44*, 805–881. [CrossRef]

22. Jin, C.; Plucknett, K.P. Microstructure instability in TiC-316L stainless steel cermets. *Int. J. Refract. Met. Hard Mater.* **2016**, *58*, 74–83. [CrossRef]